

A Coupled-Line Based L-Section DC-Isolated Dual-Band Real to Real Impedance Transformer and Its Application to a Dual-Band T-Junction Power Divider

Mohammad A. Maktoomi^{1, *} and Mohammad S. Hashmi^{1, 2}

Abstract—This paper presents a dual-band impedance transformer for real source and load impedances that is capable of providing matching at two arbitrary frequencies. There are two possible configurations of the proposed technique, and both the configurations are simple and possess flexibility to cater to wide range of impedance environments. A very useful feature of the design is its inherent ability to provide DC isolation. A prototype, which works at 1 GHz and 2 GHz, fabricated using Roger’s RO4350B laminate validates the proposed design with a good match between theoretical and experimental results. In addition, a dual-band T-junction power divider is reported to demonstrate the usefulness of the proposed impedance transformer.

1. INTRODUCTION

Impedance transformers are present in diverse RF and microwave applications irrespective of whether the applications are single-band or multi-band. Impedance transformer operating at two/multi-frequencies finds applications in the design of dual-band/multi-band amplifiers, oscillators, mixers, power splitter/combiners, antennas etc. [1–4]. Three types of matching networks are of interest to the circuit designers:

1. Real impedance to real impedance transformer.
2. Complex impedance to real impedance transformer.
3. Complex impedance to complex impedance transformer.

For example, a real to real impedance transformer is useful in power dividers [5], a complex to real impedance transformer useful in amplifiers [4], and a complex to complex impedance transformer useful in multi-stage amplifiers for inter-stage matching [6].

There have been numerous reports of dual-band matching techniques that cater to the scenarios mentioned above. For example, a transformer for providing match at a frequency and its first harmonic was reported in [7], Monzon proposed a small dual-frequency transformer to match real source and load impedances [8], whereas Chebyshev impedance transformer reported in [9, 10] and Pi-section transformer [11] also match real load impedance to real source impedance at two distinct frequencies. Furthermore, there could be a situation when the load impedance is complex as well as frequency-dependent, for instance, the input impedance of transistor while looking into its gate terminal. The design techniques reported in [12–22] pretty much address this scenario but with some limitations. For example, the technique reported in [12] provides matching between complex loads and real source impedances but does not consider frequency-dependent load. Furthermore, a three section

Received 5 November 2014, Accepted 29 November 2014, Scheduled 10 December 2014

* Corresponding author: Mohammad A. Maktoomi (ayatullahm@iiitd.ac.in).

¹ Wireless Systems Lab, Department of Electronics and Communications Engineering, IIIT Delhi, New Delhi 110020, India. ² iRadio Lab, Department of Electrical and Computer Engineering, Schulich School of Engineering, University of Calgary, Calgary, Alberta T2N 1N4, Canada.

transformer and later a generalized impedance transformer were respectively reported in [14, 15], but both of these techniques possess very complex design equations. Dual-band transformers using stub-loaded transmission line [16], T-section network [17], and dual-band line with different characteristic impedances [18] find utility in dual-band power amplifier design. A lumped components based dual-band impedance transformers was also reported [22], but it had inherent weaknesses as the operating frequency increased [6]. Recently, coupled lines have been utilized in matching complex load impedances to real source impedance [19–21, 23]. Lastly, very few tri-band/quad-band real to real impedance transformers have also been reported [24, 25].

This paper, for the first time, proposes a real to real impedance transformer capable of operating at two distinct frequencies concurrently with an inherent DC block feature. The proposed design, consisting of two sections, have been analysed to obtain closed form equations which is then simulated, fabricated, and experimentally verified. Subsequently, the usefulness of the proposed impedance transformer is demonstrated through a new dual-band T-junction power divider.

2. PROPOSED IMPEDANCE TRANSFORMER

The two proposed configurations are depicted in Figure 1. It can be seen that the only difference between these configurations is in the placement of stub. The design with stub on the load side is named as configuration-I, whereas the design with stub on the source side is named as configuration-II. The analysis of both these configurations is given in subsequent subsections.

2.1. Analysis of Configuration-I

The configuration-I is shown in Figure 1(a). It is apparent that it consists of a parallel coupled line (Section A), and a short or an open stub (Section B). In Section A, Z_e is the even-mode impedance, Z_o the odd-mode impedance, and θ_1 the electrical length of the coupled line whereas Z_2 and θ_2 are the characteristic impedance and electrical length of the stub. Y_{in1} denotes the admittance looking into Section A while Y_{in2} is the admittance looking into Section B. The physical dimensions l (length), w (width) and s (separation between coupled lines) of respective transmission-line segments are also shown in the figure. All electrical lengths are defined at the first frequency, f_1 .

As shown in [23], the value of Y_{in1} may be expressed as follows:

$$Y_{in1} = P + jQ \quad (1)$$

where, P and Q are given by (2) and (3).

$$P = \frac{4R_S(\rho - 1)^2}{4\left[R_S^2(\rho + 1)^2 - 2\rho(\rho - 1)^2 Z_o^2\right] \cos^2 \theta_1 + (\rho - 1)^4 Z_o^2 \sin^2 \theta_1 + 16\rho^2 Z_o^2 \cos^4 \theta_1 / \sin^2 \theta_1} \quad (2)$$

$$Q = \frac{\rho + 1}{Z_o} \frac{\left[4R_S^2 - (\rho - 1)^2 Z_o^2\right] \sin(2\theta_1) + 8\rho Z_o^2 \cos^3 \theta_1 / \sin \theta_1}{4\left[R_S^2(\rho + 1)^2 - 2\rho(\rho - 1)^2 Z_o^2\right] \cos^2 \theta_1 + (\rho - 1)^4 Z_o^2 \sin^2 \theta_1 + 16\rho^2 Z_o^2 \cos^4 \theta_1 / \sin^2 \theta_1} \quad (3)$$

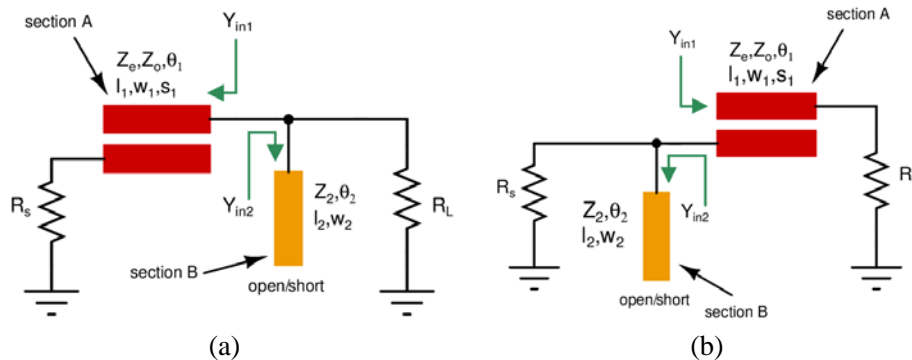


Figure 1. Proposed dual-band matching networks. (a) Configuration-I: stub on the load side. (b) Configuration-II: stub on the source side.

The factor ρ in the above expressions is the ratio, Z_e/Z_o . Equations (2) and (3) reveal that since there are only even powers of $\sin \theta_1$ and $\cos \theta_1$, the values of P will remain the same if θ_1 is replaced by $\pi - \theta_1$. Furthermore, the value of Q will change sign if θ_1 is replaced by $\pi - \theta_1$ considering that the denominator of Q contains even powers of sinusoids and that numerator has either odd-powers or $2\theta_1$ terms. With these observations, it can be concluded that $Y_{in1}|_{f_1} = Y_{in1}^*|_{f_2}$ if the value of θ_1 is given by:

$$\theta_1 = \frac{(1+q)\pi}{1+r} \quad (4)$$

where, q is an integer and r the band-ratio, f_2/f_1 .

Thus, if $Y_{in1}|_{f_1} = P + jQ$, then $Y_{in1}|_{f_2} = P - jQ$ and vice-versa.

Section A is designed in such a manner that:

$$P = 1/R_L \quad (5)$$

The imaginary part of Y_{in1} (which is $+Q@f_1$ and $-Q@f_2$) is cancelled by a dual-band susceptance (Section B) having the following property:

$$Y_{in2}|_{f_1} = -jQ \quad (6a)$$

$$Y_{in2}|_{f_2} = +jQ \quad (6b)$$

If an open stub is to be used as a dual-band susceptance, the following equations should hold true:

$$-jQ = j(1/Z_2) \tan \theta_2 \quad (7a)$$

$$+jQ = j(1/Z_2) \tan (r\theta_2) \quad (7b)$$

Simplification of (7) yields,

$$\theta_2 = \frac{(1+s)\pi}{1+r}, \text{ where } s \text{ is an Integer} \quad (8a)$$

$$Z_2 = -\tan \theta_2/Q \quad (8b)$$

Similarly, for short stub to work as a dual-band susceptance, the following equations need to be satisfied:

$$-jQ = -j(1/Z_2) \cot \theta_2 \quad (9a)$$

$$+jQ = -j(1/Z_2) \cot (r\theta_2) \quad (9b)$$

Further simplification of (9) results into:

$$\theta_2 = \frac{(1+s)\pi}{1+r}, \text{ where } s \text{ is an Integer} \quad (10a)$$

$$Z_2 = \cot \theta_2/Q \quad (10b)$$

2.2. Analysis of Configuration-II

Analysis of this configuration is similar to the previous one with the exception of the following changes.

1. R_S in Equations (2) and (3) needs to be replaced by R_L .
2. The coupled line is now designed such that

$$P = 1/R_S \quad (11)$$

3. DESIGN PROCEDURE

Design steps for the proposed network are as follows:

1. For given values of r , R_L and R_S , and assuming an appropriate value of Z_o (say, 25Ω), the value of ρ is calculated with the help of (2), (4) and (5). A realizable value of ρ lies anywhere between 2 and 4 [25]. Alternatively, assuming a suitable value for ρ , the value of Z_o can be determined using the same equations. It is reiterated that $P = 1/R_L$ or $P = 1/R_S$ needs to be set depending upon whether the configuration-I or the configuration-II is used. Thus, the corresponding value of Z_e is $\rho * Z_o$. If the obtained parameters for Section A are not physically realizable, then one needs to chose a different value for ρ and repeat the calculations.

2. Subsequently, the value of Q is evaluated with the help of (3), and using the design procedure of dual-band stubs as described previously, a suitable Section B may be designed. Practically, θ_2 is either greater or less than 90° . It is to be noticed that the value of integer s depends on the sign of Q . There are four possible cases:
 - (a) The value of Q is positive/negative and open/short stub is to be used in Section B: it follows from (8b)/(10b) that $\tan \theta_2/\cot \theta_2$ must be negative to ensure a positive value of Z_2 . This implies that the integer s must be chosen such that θ_2 comes out to be greater than 90° in (8a)/(10a).
 - (b) The value of Q is positive/negative, and short/open stub is to be used in Section B: it follows from (10b)/(8b) that $\cot \theta_2/\tan \theta_2$ must be positive as well to ensure a positive value of Z_2 . This implies that the integer s must be chosen such that θ_2 comes out to be less than 90° in (10a)/(8a).

Furthermore, the requirement to obtain physically realizable design parameters for stubs also affects the choice of integer s . Lastly, if using open stub as Section B does not yield a physically realizable l_2 and w_2 , then one will try a short stub and vice versa.

A design example shall make the procedure more clear. To that end, suppose that $R_L = 100 \Omega$ is to be matched to $R_S = 50 \Omega$ at $f_1 = 1 \text{ GHz}$ and $f_2 = 2 \text{ GHz}$ which implies $r = 2$, and thus $\theta_1 = 60^\circ$ from (4) considering $q = 0$ for compact size. Furthermore, a value of $Z_o = 25 \Omega$ is assumed. Since $P = 0.01 \text{ mho}$ from (5), the value of ρ is found from (2) which comes out to be 2.1332, omitting unreasonable values. The value of Q corresponding to $\rho = 2.1332$ is found to be 0.04639 mho from (3). Next, since the value of Q is positive, s is set as 1 in 8(a) so that $\theta_2 = 120^\circ$ and $\tan \theta_2$ becomes negative which ensures a positive value of Z_2 . The value of Z_2 evaluates to 37.34Ω from (8b). This completes the design.

Although Equation (5) along with (2) and (4) can be solved by algebraic means, a plot such as that shown in Figure 2 is very useful for a quick estimate of ρ and Q and for the intuition it may provide. For example, the question whether we can obtain a match if $R_L = 20 \Omega$ in the above example can be quickly and easily answered with the help of Figure 2(a) which clearly shows that it is not possible as the plot does not reach $P = 1/R_L = 0.05 \text{ mho}$.

4. RESULTS AND DISCUSSIONS

As a very first simulation example, it is shown that Y_{in1} is complex conjugate at the two frequencies, if θ_1 is given by (4). To that end, a coupled line with $Z_e = 75 \Omega$ and $Z_o = 25 \Omega$ is considered. Design frequencies are assumed to be $f_1 = 1 \text{ GHz}$ and $f_2 = 2 \text{ GHz}$ as an example, which corresponds to $\theta_1 = 60^\circ$. A plot of Y_{in1} for $R_S = 50 \Omega$ is shown in Figure 3. It can be readily observed that the real part is same at the two frequencies (please see the dotted line), and the imaginary part just changes its sign as the frequency goes from f_1 to f_2 (please see the two circles).

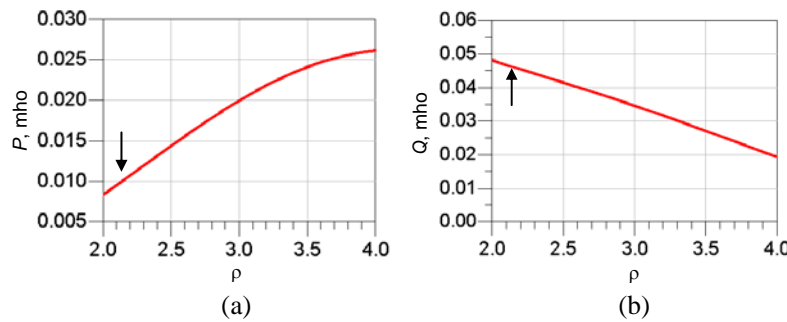


Figure 2. Variation of P and Q (@ f_1) with ρ in the above example. (a) Plot of P : arrow indicates the value of ρ ($= 2.1332$) where the value of $P = 0.01 \text{ mho}$. (b) Plot of Q : arrow indicates the value of Q corresponding to $\rho = 2.1332$.

A series of simulation is done to show the flexibility of the proposed circuits in matching different load and source impedances. It is assumed that during all these simulations the source side impedance (R_S) is 50Ω .

First, as shown in Table 1, the configuration-I is considered, and the load and f_1 are kept fixed while the value of f_2 is varied. OC denotes the use of an open circuit stub as Section B, whereas SC denotes the use of a short circuit stub. It is noticed from Table 1 that one cannot go beyond $f_2 = 3.3 \text{ GHz}$ as the value of required ρ will be greater than 4 which may pose challenges during fabrication. The corresponding return loss plots are shown in Figure 4(a).

In Table 2, the design parameters are shown for the case where the load is again fixed, but now f_1 and f_2 are both chosen arbitrarily. Figure 4(b) shows the return loss for this case.

Lastly, in Table 3, f_1 and f_2 are both held at fixed value $f_1 = 1.5 \text{ GHz}$ and $f_2 = 3 \text{ GHz}$ while the load impedance is swept. A good matching can be observed from return loss plots which appear in Figure 4(c). Again, it may be observed from Table 3 that as the value of the load impedance increases from 40Ω to 80Ω , the required value of Z_e decreases, and ultimately a situation will come ($R_L = 100 \Omega$, for example) where the required ρ will be lesser than 2.

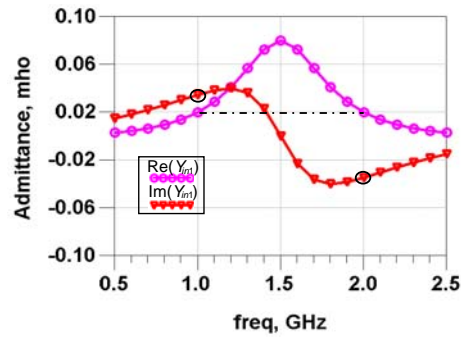


Figure 3. Variation of the real and imaginary parts of Y_{in1} . $\text{Re}(\cdot)$ returns the real part of a complex number whereas $\text{Im}(\cdot)$ returns the imaginary part.

Table 1. Configuration-I, $f_1 = 1 \text{ GHz}$, $Z_o = 25 \Omega$, $R_L = 100 \Omega$.

Cases	f_2 (GHz)	Z_e (Ω)	θ_1 (deg)	Z_2 (Ω)	θ_2 (deg)
1	2	53.33	60	37.34	120, OC
2	2.5	68.36	51.43	145.19	102.86, OC
3	3	85.36	45	44.334	45, SC
4	3.3	97.05	41.86	56.52	41.86, SC

Table 2. Configuration-I, $Z_o = 25 \Omega$, $R_L = 100 \Omega$.

Cases	f_1 (GHz)	f_2 (GHz)	Z_e (Ω)	θ_1 (deg)	Z_2 (Ω)	θ_2 (deg)
1	0.9	2.4	73.74	49.10	32.01	49.10, SC
2	1.5	3.5	63.20	54	90.15	108, OC
3	2	4.2	56.24	58.06	48.67	116.13, OC

Table 3. Configuration-I, $f_1 = 1.5 \text{ GHz}$, $f_2 = 3 \text{ GHz}$, $Z_o = 25 \Omega$.

Cases	R_L (Ω)	Z_e (Ω)	θ_1 (deg)	Z_2 (Ω)	θ_2 (deg)
1	40	91.37	60	70.10	120, OC
2	60	67.27	60	44.45	120, OC
3	80	58.48	60	39.69	120, OC

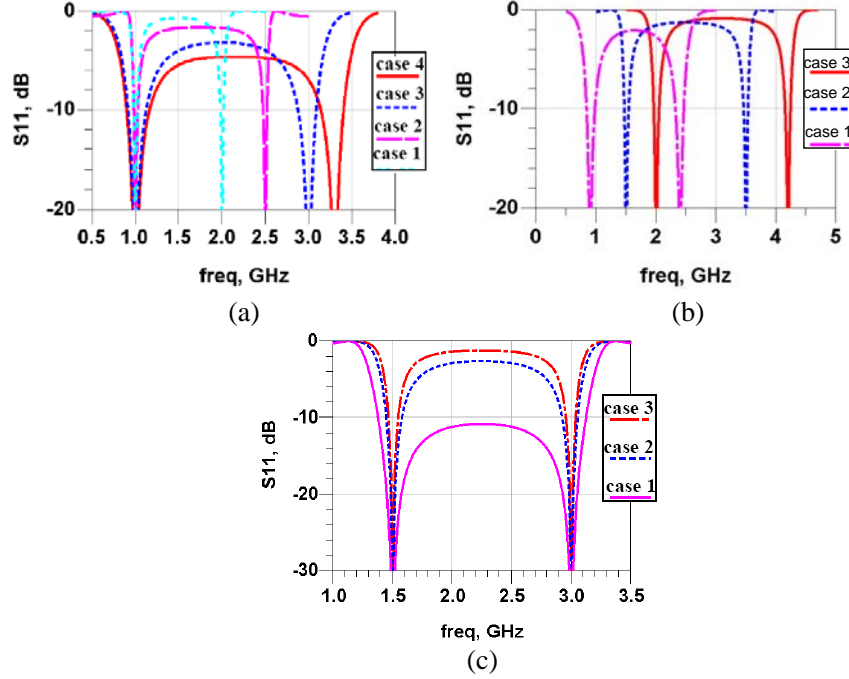


Figure 4. Return loss for the designs of (a) Table 1, (b) Table 2, (c) Table 3.

Table 4. Configuration-II, $f_1 = 1$ GHz, $Z_o = 25 \Omega$, $R_L = 20 \Omega$.

Cases	f_2 (GHz)	Z_e (Ω)	θ_1 (deg)	Z_2 (Ω)	θ_2 (deg)
1	2	53.11	60	31.37	120, OC
2	2.5	73.28	51.43	108.51	102.86, OC
3	2.9	93.61	46.15	27.60	46.15, SC

Table 5. Configuration-II, $Z_o = 25 \Omega$, $R_L = 20 \Omega$.

Cases	f_1 (GHz)	f_2 (GHz)	Z_e (Ω)	θ_1 (deg)	Z_2 (Ω)	θ_2 (deg)
1	0.8	1.8	62.50	55.38	57.17	110.76, OC
2	1.3	2.75	57.28	57.78	41.45	115.56, OC
3	2	4.5	62.50	55.38	57.17	110.77, OC
4	1.7	5.1	99.3	45	29.56	45, SC

Table 6. Configuration-II, $f_1 = 1$ GHz, $f_2 = 2$ GHz, $Z_o = 25 \Omega$.

Cases	R_L (Ω)	Z_e (Ω)	θ_1 (deg)	Z_2 (Ω)	θ_2 (deg)
1	30	58.69	60	36.80	120, OC
2	45	70.27	60	46.13	120, OC
3	65	93.86	60	67.84	120, OC

Table 4 to Table 6 show similar simulations for the configuration-II as done for configuration-I.

A comparison of the simulated results for the two configurations reveals that both of them are capable of matching quite a variety of loads at different frequencies. Perhaps, a preference in choice largely depends on the ease of fabrication.

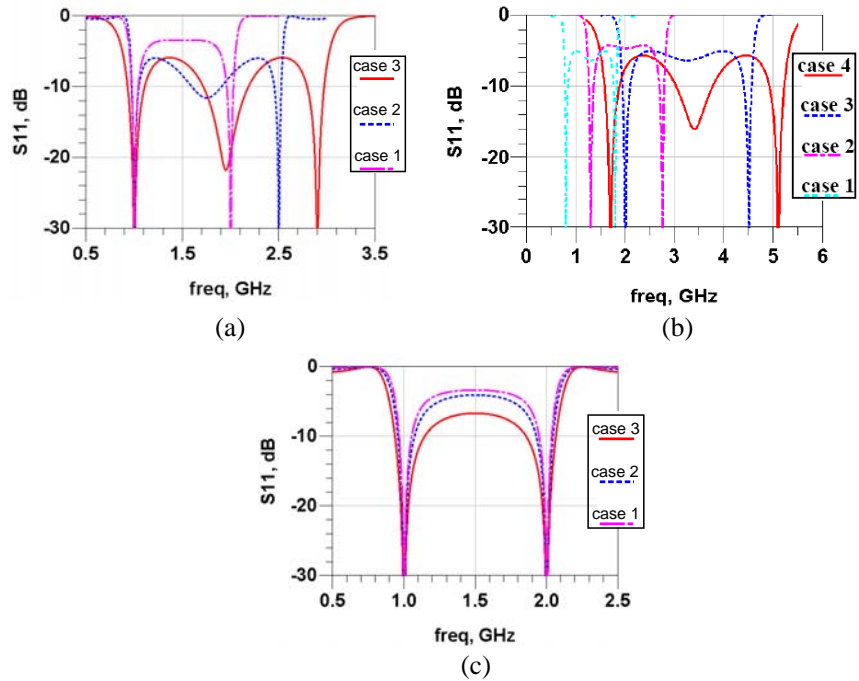


Figure 5. Return loss for the designs of (a) Table 4, (b) Table 5, (c) Table 6.

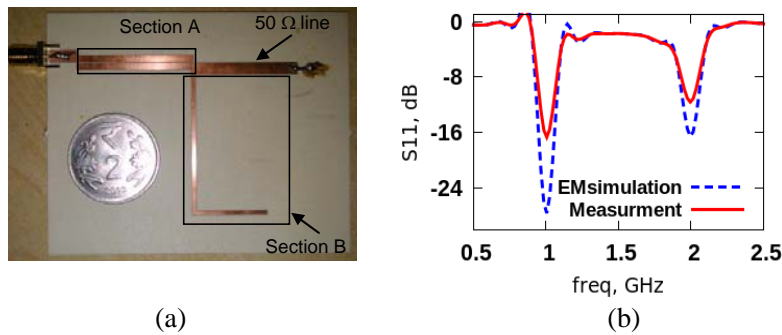


Figure 6. (a) The manufactured prototype in our lab. This is a configuration-I type matching network. (b) The measurement result as compared to the EM-simulation result.

A prototype to work at $f_1 = 1$ GHz and $f_2 = 2$ GHz is implemented for configuration-I using Roger’s RO4350B laminate on 1oz copper cladding to show the practical utility of the proposed design. The load is a 20.5Ω CRCW series SMD resistor available from Vishay. The prototype is shown in Figure 6(a) where the physical dimensions (in mm) are as follows: $l_1 = 31.620$, $w_1 = 1.750$, $s_1 = 0.285$, $l_2 = 59.517$ and $w_2 = 1.112$. The corresponding simulation and measurement results are shown in Figure 6(b).

Next, to show the practical utility of configuration-II, a T-junction power divider shown in Figure 7(a) is considered [5]. Its equivalent circuit looking from port 1 is shown in Figure 7(b). Since to have equal power division, the paths from port 1 to port 2 and from port 1 to port 3 are the same, the coupled line impedances as well as the impedance of the right-side termination gets halved in Figure 7(b). The equivalent circuit may readily be recognized as the proposed configuration-II, where the requirement is to match $R_L = Z_0/2$ to $R_S = Z_0$, where $Z_0 (= 50 \Omega)$ is the port impedance.

Based on this idea, a dual-band T-junction power divider is designed and implemented to work at $f_1 = 1$ GHz and $f_2 = 2.1$ GHz. The prototype and corresponding S -parameters are depicted in Figure 8.

It is observed from the measured result of the divider as well as from simulations depicted in Figure 4 and Figure 5 that depending upon the value of the load impedance or the design frequencies, the out-of-the-band performance may deteriorate in some cases. A remedy to circumvent this issue is to

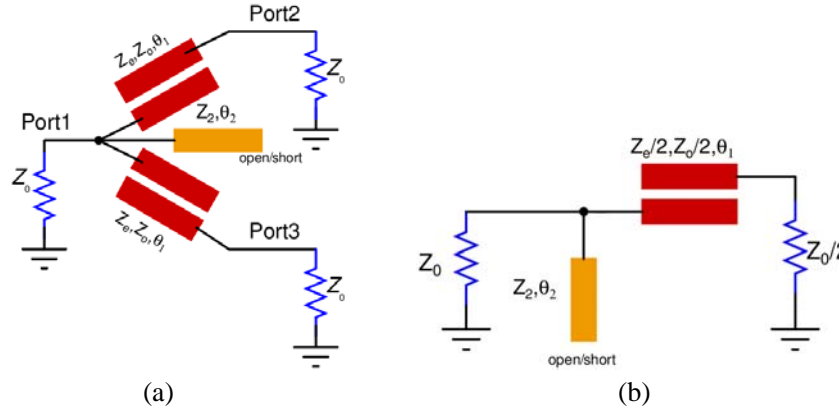


Figure 7. (a) A dual-band T-junction power divider. (b) Equivalent circuit of the divider looking into the port 1.

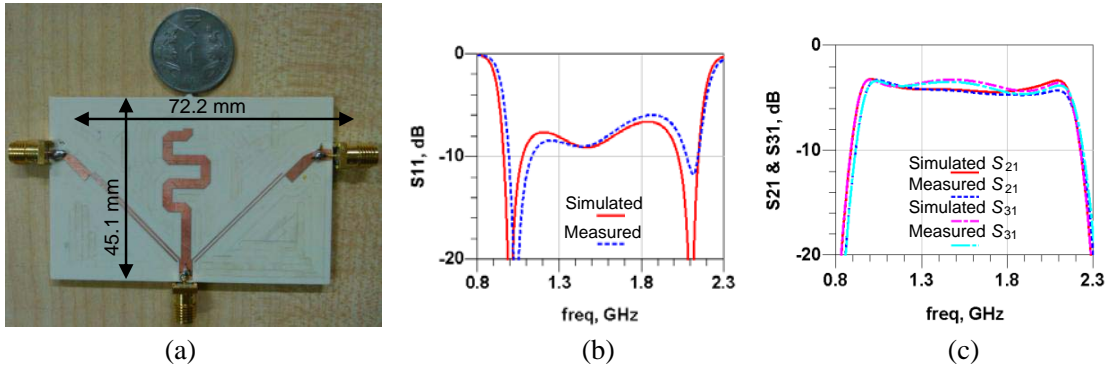


Figure 8. (a) Photograph of the designed T-junction divider. (b) Simulated/measured Return loss of port 1. (c) Simulated/measured transmissions.

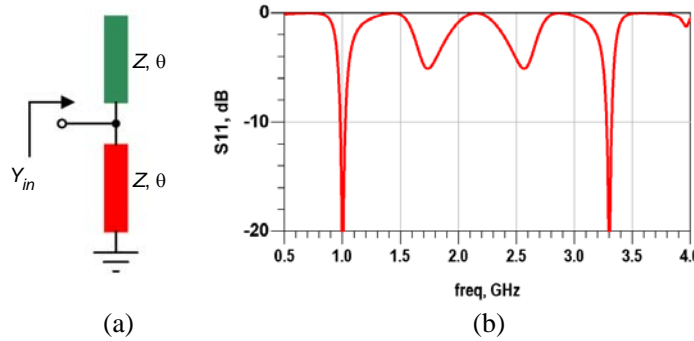


Figure 9. (a) A dual-band complex impedance using parallel combinations of open and short stubs to fine-tune out-of-the-band performance. (b) Simulated Return loss for the case4 of Table 1 showing better out-of-the-band performance.

use a parallel combination of a short and open stub shown in Figure 9(a), instead of using only either of them.

It may be proved in a manner similar to the one discussed in Section 2.1 that the value of Z is given by

$$Z = \frac{1 - \tan^2 \theta}{Q \tan \theta} \tag{12}$$

Table 7. Comparison with some existing designs.

Technique/Ref. No	Type of Load	Bands	DC Isolation	Experiment
Cascaded Transmission-Lines [8]	Real	Two	No	No
Chebyshev Function [9]	Real	Two	No	No
L-type Network [5]	Real	Two	No	Yes
Stubbed Coupled Lines [24]	Real	Three	No	Yes
Cascaded Coupled Lines [25]	Real	Four	No	Yes
This work Coupled Line + Stub	Real	Two	Yes	Yes

where, θ has the same expression as that of θ_2 .

Using this parallel stub, case 4 of Table 1 is redesigned to illustrate the improvement; the values of Z and θ are found to be $34.56\ \Omega$ and 125.58° , respectively. The simulated return loss is depicted in Figure 9(b). It is evident that the out-of-the-band performance is much better than previous result shown in Figure 4(a)/case 4. This solution would however, come at a price of increased layout complexity.

A comparison of the proposed matching network with some popular previously reported designs for real load and source impedances is presented in Table 7.

5. CONCLUSION

A dual-band impedance matching network having two possible configurations, with inherent dc blocking property, have been demonstrated. The effectiveness and flexibility of the proposed configurations have been shown through a number of simulation results. A prototype has been built to validate the performance obtained from the proposed technique. A dual-band T-junction power divider has been proposed as an example application of the developed impedance transformer.

REFERENCES

1. Rawat, K., M. S. Hashmi, and F. M. Ghannouchi, "Dual-band RF circuits and components for multi-standard software defined radios," *IEEE Circuits & Systems Magazine*, Vol. 12, No. 1, 12–32, First Quarter 2012.
2. Hashemi, H. and A. Hajimiri, "Concurrent multiband low-noise amplifiers — Theory, design, and applications," *IEEE Transactions on Microwave Theory and Techniques*, Vol. 50, No. 1, 288–301, Jan. 2002.
3. Nallam, N. and S. Chatterjee, "Multi-band frequency transformations, matching networks and amplifiers," *IEEE Transactions on Circuits & Systems I: Reg. Papers*, Vol. 60, No. 6, 1635–1647, Jun. 2013.
4. Iyer, B. and N. P. Pathak, "A concurrent dual-band LNA for noninvasive vital sign detection system," *Wiley Microwave & Optical Technology Letters*, Vol. 56, No. 2, 391–394, Feb. 2014.
5. Park, M. J. and B. Lee, "Dual band design of single stub impedance matching networks with application to dual band stubbed T junctions," *Wiley Microwave & Optical Technology Letters*, Vol. 52, No. 6, 1359–1362, 2010.
6. Hsieh, K.-A., H.-S. Wu, K.-H. Tsai, and C.-K. C. Tzuang, "A dual-band 10/24-GHz amplifier design incorporating dual-frequency complex load matching," *IEEE Transactions on Microwave Theory and Techniques*, Vol. 60, No. 6, 1649–1657, Jun. 2012.
7. Chow, Y. L. and K. L. Wan, "A transformer of one-third wavelength in two sections — For a frequency and its first harmonic," *IEEE Microwave and Wireless Components Letters*, Vol. 12, No. 1, 22–23, Jan. 2002.
8. Monzon, C., "A small dual-frequency transformer in two sections," *IEEE Transactions on Microwave Theory and Techniques*, Vol. 51, No. 4, 1157–1161, Apr. 2003.
9. Sophocles, J. and A. Orfanidis, "Two-section dual-band Chebyshev impedance transformer," *IEEE Microwave and Wireless Components Letters*, Vol. 13, No. 9, 382–384, Sep. 2003.

10. Castaldi, G., "An exact synthesis method for dual-band Chebyshev impedance transformers," *Progress In Electromagnetics Research*, Vol. 86, 305–319, 2008.
11. Wu, Y., Y. Liu, and S. Li, "A compact Pi-structure dual band transformer," *Progress In Electromagnetics Research*, Vol. 88, 121–134, 2008.
12. Wu, Y., Y. Liu, and S. Li, "A dual-frequency transformer for complex impedances with two unequal sections," *IEEE Microwave and Wireless Components Letters*, Vol. 19, No. 2, 77–79, Feb. 2009.
13. Giannini, F. and L. Scucchia, "A complete class of harmonic matching networks: Synthesis and application," *IEEE Transactions on Microwave Theory and Techniques*, Vol. 57, No. 3, 612–619, Mar. 2009.
14. Liu, X., Y. Liu, S. Li, F. Wu, and Y. Wu, "A three-section dual-band transformer for frequency-dependent complex load impedance," *IEEE Microwave and Wireless Components Letters*, Vol. 19, No. 10, 611–613, Oct. 2009.
15. Wu, Y., Y. Liu, S. Li, C. Yu, and X. Liu, "A generalized dual-frequency transformer for two arbitrary complex frequency-dependent impedances," *IEEE Microwave and Wireless Components Letters*, Vol. 19, No. 12, 792–794, Dec. 2009.
16. Chuang, M.-L., "Dual-band impedance transformer using two-section shunt stubs," *IEEE Transactions on Microwave Theory and Techniques*, Vol. 58, No. 5, 1257–1263, May 2010.
17. Nikravan, M. A. and Z. Atlasbaf, "T-section dual-band impedance transformer for frequency-dependent complex impedance loads," *Electronics Letters*, Vol. 47, No. 9, 551–553, Apr. 28, 2011.
18. Rawat, K. and F. M. Ghannouchi, "Dual-band matching technique based on dual-characteristic impedance transformers for dual-band power amplifiers design," *IET Microwaves, Antennas & Propagation*, Vol. 5, No. 14, 1720–1729, Nov. 18, 2011.
19. Wu, Y., W. Sun, S.-W. Leung, Y. Diao, and K.-H. Chan, "A novel compact dual-frequency coupled-line transformer with simple analytical design equations for frequency-dependent complex load impedance," *Progress In Electromagnetics Research*, Vol. 134, 47–62, 2013.
20. Li, S., B. Tang, Y. Liu, S. Li, C. Yu, and Y. Wu, "Miniaturized dual-band matching technique based on coupled-line transformer for dual-band power amplifiers design," *Progress In Electromagnetics Research*, Vol. 131, 195–210, 2012.
21. Wu, Y., Y. Liu, S. Li, and C. Yu, "New coupled-line dual-band dc-block transformer for arbitrary complex frequency-dependent load impedance," *Wiley Microwave & Optical Technology Letters*, Vol. 54, No. 1, 139–142, Jan. 2012.
22. Moon, B.-T. and N.-H. Myung, "A dual-band impedance transforming technique with lumped elements for frequency-dependent complex loads," *Progress In Electromagnetics Research*, Vol. 136, 123–139, 2013.
23. Maktoomi, M. A., M. S. Hashmi, and F. M. Ghannouchi, "A T-section dual-band matching network for frequency-dependent complex loads incorporating coupled line with DC-block property suitable for dual-band transistor amplifiers," *Progress In Electromagnetics Research C*, Vol. 54, 75–84, 2014.
24. Wang, X. H., L. Zhang, Y. Xu, Y. F. Bai, C. Liu, and X.-W. Shi, "A tri-band impedance transformer using stubbed coupling line," *Progress In Electromagnetics Research*, Vol. 141, 33–45, 2013.
25. Bai, Y.-F., X.-H. Wang, C.-J. Gao, Q.-L. Huang, and X.-W. Shi, "Design of compact quad-frequency impedance transformer using two-section coupled line," *IEEE Transactions on Microwave Theory and Techniques*, Vol. 60, No. 8, 2417–2423, Aug. 2012.